Journal of Earthquake Engineering

ISSN: 1363-2469 (Print) 1559-808X (Online) Journal homepage: www.tandfonline.com/journals/ueqe20

A Shake Table Study on Caster Configuration in the Seismic Response of Rolling Equipment

Cong Xu, Quincy T. Ma, Sherif Beskhyroun & Masahiro Kurata

To cite this article: Cong Xu, Quincy T. Ma, Sherif Beskhyroun & Masahiro Kurata (12 Jul 2025): A Shake Table Study on Caster Configuration in the Seismic Response of Rolling Equipment, Journal of Earthquake Engineering, DOI: 10.1080/13632469.2025.2525923

To link to this article: https://doi.org/10.1080/13632469.2025.2525923

JOURNAL OF EARTHQUAKE ENGINEERING
https://doi.org/10.1080/13632469.2025.2525923

Taylor & Francis
Taylor & Francis Group

A Shake Table Study on Caster Configuration in the Seismic Response of Rolling Equipment

Cong Xu [a], Quincy T. Ma [a], Sherif Beskhyroun [b], and Masahiro Kurata [c]

[a]Department of Civil & Environmental Engineering, The University of Auckland, Auckland, New Zealand; [b]School of Future Environments, Auckland University of Technology, Auckland, New Zealand; [c]Disaster Prevention Research Institute, Kyoto University, Kyoto, Japan

ABSTRACT

This study investigates the seismic performance of equipment on casters through over 1,300 shake table tests, focusing on different caster locking conditions and their effects on trolley motion. Using motion capture, accelerometers, and video recordings, the study accurately monitored specimen movement and caster dynamics. Results showed locking two diagonal casters led to best rolling characteristics that minimizes accelerations and displacements on balance. Twin-wheel casters specially designed for medical applications outperformed conventional single-wheel casters. A linear relationship was established for estimating peak rolling response, offering a practical method for engineers to assess seismic performance of rolling equipment.

ARTICLE HISTORY
Received 30 October 2024
Accepted 4 June 2025

KEYWORDS
Shake table testing; non-structural elements (NSEs); medical equipment; rolling object on casters; building contents

1. Introduction

Damage to non-structural elements (NSEs) can lead to significant economic losses, reduced building functionality, and increased risk of casualties and fatalities following earthquakes (Mitrani-Reiser et al. 2012; Taghavi and Miranda 2003). In many buildings, especially medical facilities, NSEs and contents represent a significant portion of the total investment, sometimes as much as 90% (Taghavi and Miranda 2003). Good seismic performance of NSE is crucial for maintaining the operational functionality of medical facilities in the aftermath of an earthquake (Mayer and Boston 2022; Miranda et al. 2012). Damaged NSEs and displaced contents can impede safe evacuation, posing risks to building occupants or patients and staff in a hospital context (Suzuki, Fukuda, and Nakaji 2014; Zhang et al. 2012).

Observations from past earthquakes indicate that even when structural systems sustain minor damage, NSEs and building contents can be significantly affected (Applied Technology Council 2015; Dhakal 2010). The economic impact of damaged NSEs often exceeds that of structural damage (Fajfar and Krawinkler 2004; Filiatrault and Sullivan 2014). For instance, following the 2010 Chile earthquake, approximately 62% of hospitals in the affected area required repairs due to non-structural damage, and around 75% of hospital elevators were non-functional (Miranda et al. 2012). Despite advancements in understanding the seismic performance of NSEs and building contents, significant damage was still reported in Wellington, New Zealand after the 2016 Kaikōura earthquake (Baird and Ferner 2017).

The present study focuses on the seismic performance of rolling equipment supported on casters. Nikfar and Konstantinidis (2019) differentiate wheels and casters by their movements. Wheels rotate around a fixed horizontal axle, while casters can both rotate around a horizontal axle and swivel

CONTACT Cong Xu cxu413@aucklanduni.ac.nz Department of Civil & Environmental Engineering, The University of Auckland, Engineering Block 1 - Bldg 401, 20 Symonds St, Auckland 1010, New Zealand

around a vertical axis. The seismic response of castered objects remains a critical yet underexplored area, particularly concerning medical equipment which is often mounted on casters without anchorage (Myrtle et al. 2005). Essential life preserving medical devices like intensive care unit (ICU) monitoring systems, anesthesia equipment, ventilators, medicine infusion/syringe pump and defibrillators are typically castered and freestanding. They are thus vulnerable to damage from collisions or overturning during earthquakes (Ornthammarath and Puavaranukroh 2018). Existing research primarily addresses the seismic performance of stationary contents without casters (Di Sarno et al. 2019). Another approach has been to consider wheels and casters as sliding objects (Dhakal et al. 2016; Yeow et al. 2018). However, not many studies adequately consider castered objects' unique responses due to their mobility (Guamán-Cabrera, De La Llera, and Mery 2023; Wang, Dai, and Ning 2016).

Despite the prevalence of casters in medical facilities, research on this topic remains limited. These types of elements are typically subjected to dynamic experimental testing procedures (Zito et al. 2022). Noteworthy studies include:

- Testing of a B-ultrasound room with various contents, both with and without casters (Wang, Dai, and Ning 2016).
- Tests of a five-story building with the top two floors configured as a surgery suite and intensive care unit (Pantoli et al. 2013).
- Shake table tests of seismic restraints for various medical equipment (Chai and Lin 2011), and
- Tests examining medical equipment with both locked and unlocked casters (Nikfar and Konstantinidis 2019).

These studies mainly address specific typical hospital room contents, highlighting a gap for a systematic investigation into the key factors affecting rolling response, such as mass distribution, wheel material, caster configuration and caster locking conditions.

This study presents a shake table test program using a specifically designed configurable trolley to emulate various commonly used castered medical equipment. The trolley allow flexible change in casters, specimen mass, and center of mass. The tests specifically investigated seven caster locking conditions under a purposefully selected set of table motions.

2. Shake Table Test Design

This investigation included over 1,300 unidirectional shake table test runs exploring a wide range of configurations. This included five caster types, six initial wheel angles, three trolley orientations, three self-weight variations, three center of mass heights, and seven caster locking conditions, across sixteen different ground motions.

The experiment setup consisted of a custom trolley (described later), positioned on a 4 mm thick vinyl floor covering glued to a stiff plywood sheet over an steel table surface. The selected flooring is a commercial product commonly used in healthcare environments. The flooring was professionally installed by flooring contractors with a 2 mm gauge and a 2 mm wearing layer. The overall testing setup is illustrated in Fig. 1.

2.1. Instrumented Trolley for Simulating Rolling Medical Equipment

The rolling specimen for the shake table experiment is a steel trolley weighing 97 kg as shown in Fig. 2. The trolley's dimensions are 1100 × 550 x 1470 mm (B x D x H), with its center of mass located at the planar geometric center, 487 mm above the base plate. Additional components include a concrete block holder on the middle shelf and an anti-overturning timber outrigger below the base plate. These bring the specimen's total mass to 122 kg, with the final center of mass height dependent on caster selection. Whilst this may appear heavy, but heavy medical equipment is common in hospitals. For example, anesthesia machines typically weigh over 120 kg, blood plasma freezers range between

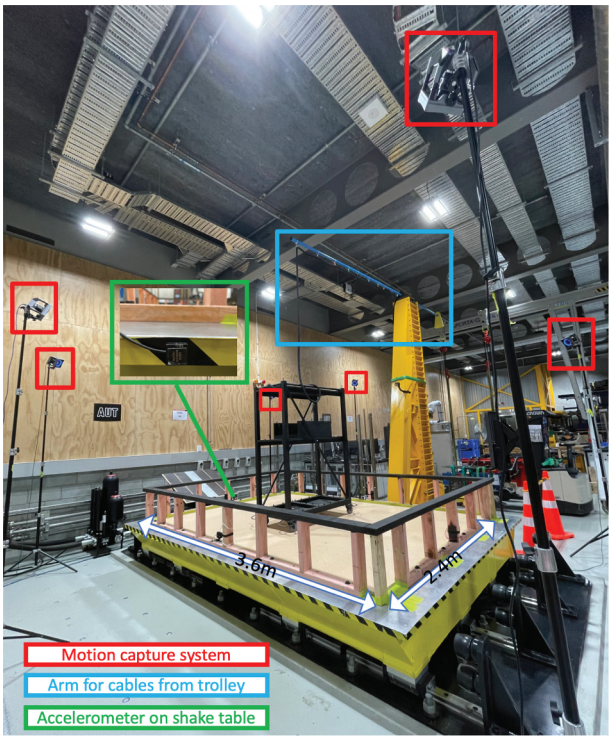

Figure 1. Overall layout of the shake table experiment.

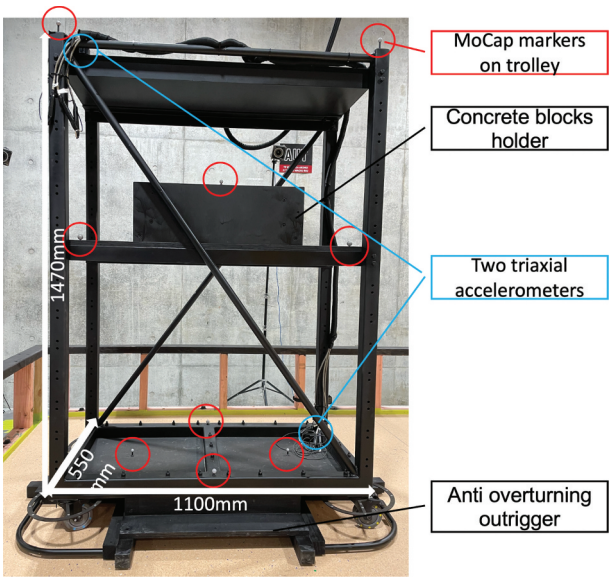

Figure 2. Trolley specimen used for shake table tests.

160–190 kg, and autoclaves can weigh 360 kg or more. To prevent interference with the Motion Capture (MoCap) system, the trolley and the casters are coated in a matte black finish.

Figure 3. Reflective markers on a disk fixed to caster's fork (left), and disk mounted to the plate-type caster (middle) or stem-type caster (right).

2.2. Instrumentation System

2.2.1. Motion Capture System

The experiment employs a Motion Capture (MoCap) system to measure the three-dimensional displacement and rotation of the trolley and the casters. This MoCap system consists of six OptiTrack Prime41 cameras strategically positioned around the shake table, reflective targets in the form reflective target balls or reflective stickers, and OptiTrack's proprietary software, Motive, for synchronizing data streams and performing computer vision calculations (OptiTrack 2023). The MoCap system simplifies instrumentation and does not interfere with the specimen's motion.

Reflective markers or stickers are placed at various points on the trolley body and the casters. The forks of each caster are fitted with a plastic disc with distinct patterns of reflective stickers (see Fig. 3). These distinct patterns aid Motive to identify and track individual casters during testing.

2.2.2. Accelerometers

Two tri-axial accelerometers were mounted on the trolley, one at the top and one at the base, as marked by the blue circles in Fig. 2. Additionally, a single-axis accelerometer on the shake table recorded its motion. All cables were suspended above the trolley and routed through a rotating arm to prevent interference with the trolley's movement. The accelerometer data were synchronized with the MoCap data through triggered sampling.

2.2.3. Conventional Video Recording

In addition to the MoCap system, six GoPro cameras were strategically positioned to capture the rolling motion of the individual casters. Four of these cameras were mounted on the table and focused on the lower part of the trolley to record wheel motion, while the other two were positioned at elevated angles off the shaking table to provide a wider field of view of the tests, as shown in Fig. 4.

Figure 4. Video captured by six GoPro cameras.

Table 1. Summary of factors evaluated in shake table tests.

Caster (Table 2)			Payload (Table 3)		Orientation (Figure 8)		
Wheel Material	Wheel diameter (mm)	Ground Motion (Table 4)	Additional mass	Mid shelf height	Wheel angle	Trolley angle	Lock Caster (Figure 7)
Institutional Rubber, Polyurethane nylon	100, 125	GM1-GM16	Low, Med, High	Low, Mid, High	0, 45, 90, 180, 0 + 45, 0 + 90	0, 45, 90	Seven different arrangements

2.3. Testing Variables and Parameters

Table 1 summarizes the parameters underpinning the test combinations for this test series.

2.3.1. Casters

Five distinct types of casters were utilized in the shake table tests, as shown in Fig. 5, with their detailed specifications provided in Table 2. The casters tested varied in,

- Wheel size (100 mm or 125 mm diameter)
- Materials (institutional rubber or polyurethane), and
- Style
  (a) Types 1, 3 and 4 casters can swivel and are mounted via a plate,
  (b) Type 2 caster is a rigid caster mounted via a plate and does not swivel,
  (c) Type 5 caster is a unique swiveling twin-wheel, stem-mounted caster, typically used in medical applications.

Type 1 casters were designated as the reference group, for comparative analysis with the other casters that varied in wheel sizes and materials.

2.3.2. Trolley Weight and Centre of Mass Height

The trolley specimen featured a central shelf adjustable to different heights. For the tests, we selected three configurations, "L" (Low), "M" (Medium), and "H" (High), as shown in Fig. 6.

Different system mass scenarios were created by placing none, two, or four concrete blocks (each with a mass of 13.6 kg) onto the central shelf. This resulted in three levels of trolley self-weight, designated as "L" (Low), "M" (Medium), and "H" (High) (details presented in Table 3, and shown graphically in Fig. 6). Considering the three levels of trolley weight and the three center of mass heights, a total of nine unique combinations were created for the shake table tests.

2.3.3. Casters Locking Conditions

Figure 7 illustrates the seven different caster locking configurations tested in this project:

Table 2. Caster information.

ID	Caster	Single or Twin Wheel	Diameter (mm)	Width (mm)	Rigid or Swivel	Wheel Material	Swivel Offset (mm)	Height (mm)
1	R100si.	S	100	32	S	Institutional Rubber	84	131
2	R100ri.	S	100	32	R	Institutional Rubber	-	131
3	R125si	S	125	32	S	Institutional Rubber	100	160
4	P100si	S	100	32	S	Polyurethane	84	131
5	Med	T	100	2x16	S	Polyurethane	80	123

Figure 5. Casters used in the shake table tests. #1 to #5 from left to right.

Figure 6. Adjustable center of mass by changing middle shelf position, "L," "M," and "H" from left to right.

Table 3. Three trolley's self-weight levels.

Trolley Mass	Concrete Block Mass (kg)	Total Mass (kg)	Self-Weight Level
122 kg	0	122	L
	2 x13.6	149	M
	4 x13.6	176	H

(1) Free rolling, with no locked casters (L0),
(2) Locking a single caster (L1),
(3) Locking two casters on the trolley's short side (L2S),
(4) Locking two casters on the trolley's long side (L2L),
(5) Locking two diagonal casters (L2D),
(6) Locking three casters (L3), and
(7) Locking all four casters (L4).

2.3.4. Wheel and Trolley Angles

The experiments involved varying the wheel and trolley angles relative to the direction of ground motion, as illustrated in Fig. 8. Nine wheel angle configurations were tested, namely

- Four cases when all four casters were set at 0, 45, 90, and 180 degrees to the excitation direction.
- Three cases with two rigid and two swivel casters, where the swivel casters were initially orientated at 0, 45 and 90 degrees.
- Two cases where two casters were set at 0 degrees and the others at either 45 or 90 degrees.

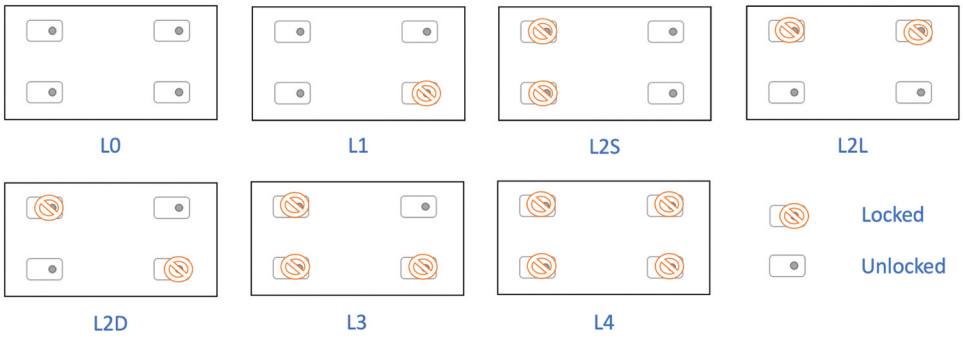

Figure 7. Considered caster locking conditions.

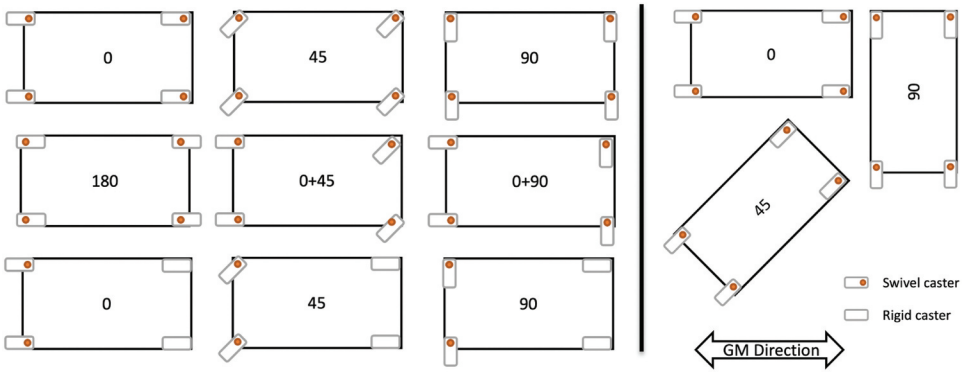

Figure 8. Nine wheel angles configurations (left) and three trolley angles (right) tested.

Figure 8 (right) shows the three trolley angles that were tested. For simplicity, the figure only depicts the three fundamental configurations with the wheel angle consistently set at 0 degree relative to the trolley body. Other tests also considered cases where wheel angles are at 45 degree.

2.3.5. Selected Ground Motions

The shake table tests in this study utilized 16 ground motions, each tested at two different intensities. These included:

- Three sets of sinusoidal motions at 1, 3 and 5 Hz,
- Two sets of sweeping sinusoidal motions from 0.5 to 8 Hz, and
- Three sets of recorded earthquake motions, namely motion from 1995 Kobe, 2011 Christchurch and 1940 El Centro earthquakes.

The earthquake records were specifically selected to ensure a variety of frequency content and strong shaking duration. Earthquake records were also selected for their familiarity to the earthquake engineering community.

Table 4 details the key parameters for these table motions, and Fig. 9 illustrates their time histories. A ramp is applied during the first 5 seconds of the six sinusoidal ground motions to avoid an abrupt start. Duration refers to the total duration of ground shaking.

Table 4. Key parameter of ground motions selected for shake table tests.

	Ground Motion	a_{max} (g)	v_{max} (mms^{-1})	d_{max} (mm)	Duration (s)
GM01	Sine, 1 Hz, 0.2 g	0.20	312	50	60
GM02	Sine, 1 Hz, 0.5 g	0.50	781	124	60
GM03	Sine, 3 Hz, 0.5 g	0.50	262	14	60
GM04	Sine, 3 Hz, 1 g	1.00	520	28	60
GM05	Sine, 5 Hz, 0.5 g	0.50	156	5	60
GM06	Sine, 5 Hz, 1 g	1.00	312	10	60
GM07	Sweep sine, f = 0.5-2 Hz	0.20	624	200	60
GM08	Sweep sine, f = 2–0.5 Hz	0.20	624	200	60
GM09	Sweep sine, f = 2-8 Hz	1.00	772	62	60
GM10	Sweep sine, f = 8-2 Hz	1.00	772	62	60
GM11	1995 Kobe KJMA, 0, 50%	0.42	456	105	60
GM12	1995 Kobe, KJMA, 0, 100%	0.83	911	211	60
GM13	2011 Christchurch, CBGSN89W, 50%	0.28	283	130	45
GM14	2011 Christchurch, CBGSN89W 90%	0.50	510	234	45
GM15	1940 El Centro, 180, 50%	0.14	155	43	54
GM16	1940 El Centro, 180, 100%	0.28	309	87	54

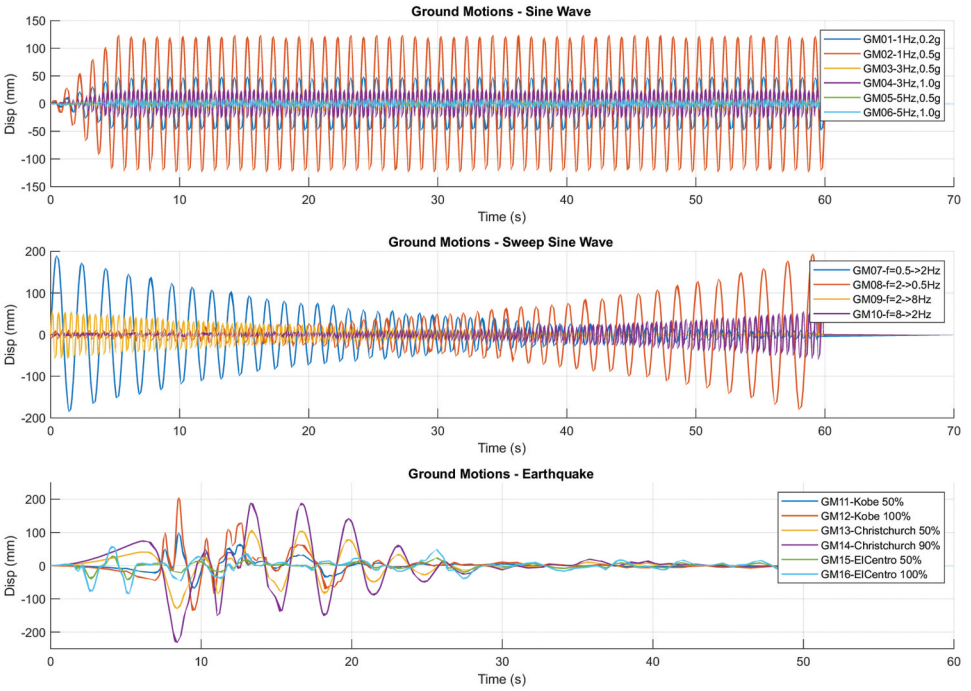

Figure 9. Ground motions for the shake table tests.

2.4. Factors Investigated in This Study

This study principally investigates the effect of caster locking conditions on the seismic response of rolling equipment. Other factors, such as trolley weight and wheel angle, are significant on their own and will be addressed in future studies. For this investigation, ground motions from the Kobe and Christchurch earthquakes, each applied at two scaling levels, were used. Other shake table inputs, including sinusoidal motion, were not suited for examining caster locking effects and will instead be used to in future studies to investigate the influence of other parameters.

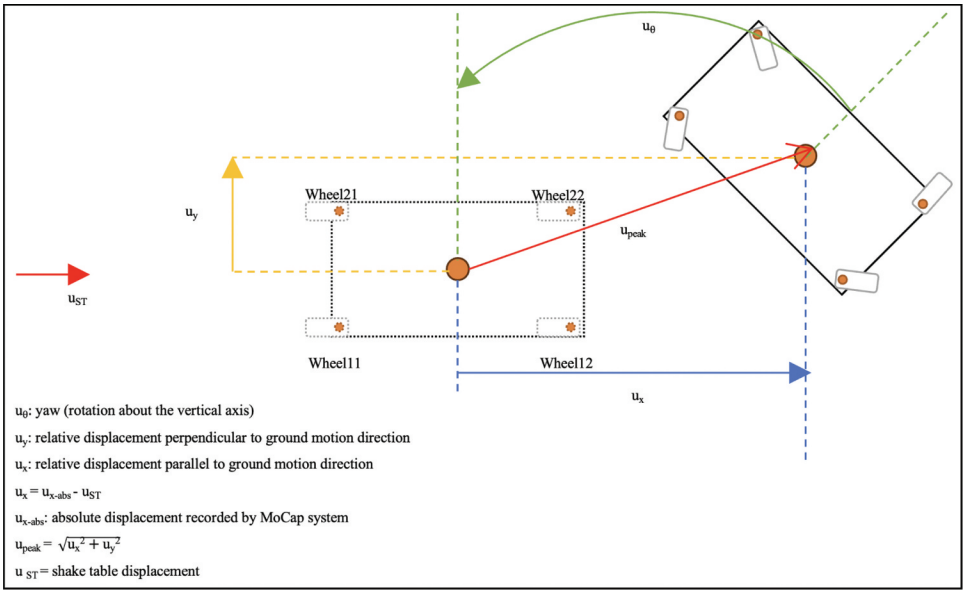

Figure 10. Variable definition of trolley motion.

Figure 10 shows the relative displacement, absolute displacement, peak displacement, and planar rotation definitions. It is worth noting that acceleration data is measured in total acceleration.

3. Effect of Locking Conditions on Rolling Equipment Seismic Response – Experimental Observation

This study examines seven different caster locking strategies as shown in Fig. 7. When a caster is locked, both the rolling of the caster wheel and the twisting of the caster are restricted. Locking eliminates rolling and twisting motions and restrict a caster to slide at the point of contact. When casters are locked, there may be still a slight degree of wheel rolling, especially under larger earthquake conditions.

Approximately 300 of the total 1,302 tests were conducted to examine the impact of locking conditions. Table 5 summarizes the testing matrix for these factors.

3.1. Overall Response

Figure 11 provides an overview of the peak and residual trolley response across the various combinations considered in this project. Each bar represents the average peak response (displacement, velocity or accelerations) from six repeated trials for each parameter combination. Note that the L3 and L4

Table 5. Testing matrix for comparing seven locking conditions.

Caster	Ground motion	Wheel angle (deg.)	Weight levels	Lock	Trolley angle (deg.)	Middle shelf height
R100si, Med	Kobe 50%, Kobe 100%, Christchurch 50%, Christchurch 90%	0	L	Seven arrangements as shown in Figure 7	0, 45, 90	M

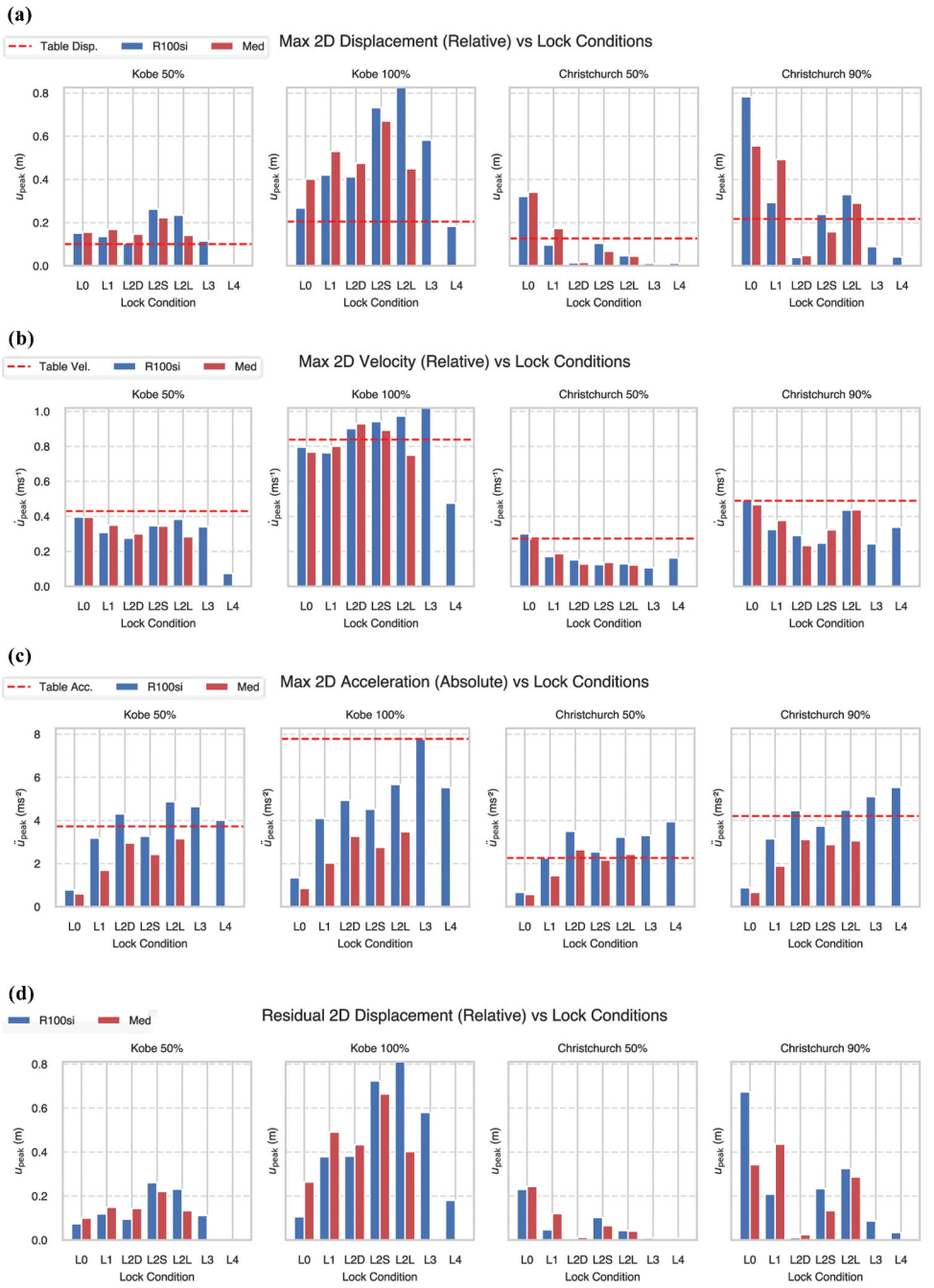

Figure 11. Mean peak trolley displacement (a), velocity (b), acceleration (c) and residual displacement (d) data for two types of casters, under different ground motions and various locking conditions.

combinations (locking three and four casters) were not tested with the Medical casters, as only two casters with brakes were available for this study.

Figure 11 presents the overall trolley response under various locking conditions. Generally, as more caster wheels are locked, the specimen's acceleration increases. Velocity, however, remains relatively consistent across all locking conditions. Displacement is minimized when

three or four casters are locked, but no clear pattern is observed for displacement when one or two casters are locked. This can be explained by the transition from free rolling to constrained movement, where the locked casters introduce resistance, causing more sliding than rolling. The residual responses closely correlated with the peak displacements. This behavior likely arises because large displacement cycles, particularly those caused by sudden jolts, effectively reset the cart's reference position, shifting its equilibrium point toward the peak displacement. Outside of these large excursions, the cart exhibits minimal additional movement resulting in residual displacement matching the peak displacement during the high-amplitude cycles. Additionally, Fig. 11 shows that all caster types follow a similar trend in peak responses. The specific results for each locking condition are as follows:

Free rolling condition (L0):

- Exhibits the lowest acceleration response among all locking conditions. In this arrangement, the trolley appears to "float" and remaining stationary in space while the floor moves back-and-forth beneath it.
- Under Christchurch earthquake excitation, this locking condition results in the largest trolley displacement. However, this did not occur during the Kobe excitations (GM11 & GM12) and the displacement remained small compared to other locking conditions.

Lock one caster (L1):

- Shows the second lowest acceleration response but experiences significant displacement amplification.

Lock two casters on long size (L2L) and Lock two casters on short size (L2S):

- Both configurations demonstrate moderate acceleration responses but large displacement responses.

Lock two casters on the diagonal (L2D):

- Characterized by low to moderate acceleration and displacement responses.
- Produces the smallest displacement under Christchurch motion (GM13 & GM14) and shows displacement comparable to L1 under Kobe motion (GM11 & GM12).

Lock three casters (L3) and Lock four (all) casters (L4):

- The L4 condition exhibits the smallest relative displacement but at the expense of the highest acceleration response. Under high PGA ground motion, the trolley experiences severe sliding and unstable rocking.

An interesting observation is that trolley displacement paradoxically increase as the system transition from free rolling to locked caster. This can be explained by accounting for recentering behavior. Under free-rolling condition, the specimen recenters almost fully in response to the cyclical ground motion. However, when casters are locked, the system may exhibit ratcheting behavior, where displacement is not fully reversed each cycle, resulting in cumulative rotation and progressively larger displacements as the motion continues.

Table 6. Trolley response amplification factor of each ground motion and locking condition.

		Acceleration amplification (R_a)				Velocity amplification (R_v)				Displacement amplification (R_d)			
Ground Motion→		Kobe 50%	Kobe 100%	ChCh 50%	ChCh 90%	Kobe 50%	Kobe 100%	ChCh 50%	ChCh 90%	Kobe 50%	Kobe 100%	ChCh 50%	ChCh 90%
Locking Conditions	L0	0.18	0.14	0.27	0.18	0.92	0.93	1.04	0.97	1.53	1.67	2.62	3.06
	L1	0.66	0.4	0.82	0.6	0.77	0.93	0.65	0.72	1.52	2.33	1.07	1.8
	L2D	0.98	0.53	1.36	0.9	0.67	1.08	0.51	0.54	1.24	2.14	0.11	0.2
	L2L	1.06	0.6	1.25	0.9	0.78	1.02	0.46	0.89	1.87	3.18	0.36	1.42
	L2S	0.77	0.47	1.05	0.8	0.81	1.09	0.48	0.6	2.42	3.43	0.68	1.03
	L3	1.25	1	1.45	1.21	0.79	1.21	0.39	0.5	1.14	2.84	0.09	0.41
	L4	1.35	0.71	1.75	1.31	1.08	0.57	0.59	0.69	0.69	0.9	0.09	0.19

3.2. Response Amplification Factors

3.2.1. Methodology

Three response amplification factors (R_d, R_v, and R_a) were defined and evaluated to assess the effectiveness of each locking configuration in isolating the input motion. These factors were calculated, collated, and ranked for each configuration across the ground motion series. The results are summarized in Table 6 for the response amplification factors and in Table 7 for the ranking. They are calculated as the average of two repeated tests and two casters for each lock condition and ground motion. The definition of u_{peak} is shown in Fig. 10, and PGD, PGV and PGA are peak ground displacement, velocity and acceleration respectively:

- $R_d = u_{peak}/\mathrm{PGD}$
- $R_v = \dot{u}_{peak}/\mathrm{PGV}$
- $R_a = \ddot{u}_{peak}/\mathrm{PGA}$

Table 7 ranks each locking condition based on how it amplifies acceleration, velocity, and displacement across the four ground motions. The amplification levels are shown as $R_{a\text{-}rank}$, $R_{v\text{-}rank}$ and $R_{d\text{-}rank}$, representing the rankings for acceleration, velocity, and displacement amplification, respectively.

Summing these ranks for each locking condition produces the values in the SUM column in Table 7. This effectively applies an equal weighting (factor of 1) to acceleration, velocity, and displacement and does not account for minimizing a specific parameter. Greater flexibility can be achieved by applying different weights to each factor: W_a for acceleration, W_v for velocity, and W_d for

Table 7. Trolley response amplification factor rank of each ground motion and locking condition.

		$R_{a\text{-}rank}$				$R_{v\text{-}rank}$				$R_{d\text{-}rank}$				
Ground Motion →		Kobe 50%	Kobe 100%	ChCh 50%	ChCh 90%	Kobe 50%	Kobe 100%	ChCh 50%	ChCh 90%	Kobe 50%	Kobe 100%	ChCh 50%	ChCh 90%	SUM
Locking Conditions	L0	1	1	1	1	6	2	7	7	5	2	7	7	47
	L1	2	2	2	2	2	2	6	5	4	4	6	6	43
	L2D	4	4	5	4	1	5	4	2	3	3	3	2	40
	L2L	5	5	4	4	3	4	2	6	6	6	4	5	54
	L2S	3	3	3	3	5	6	3	3	7	7	5	4	52
	L3	6	7	6	6	4	7	1	1	2	5	1	3	49
	L4	7	6	7	7	7	1	5	4	1	1	1	1	48
Note		Rank 1 represents the lowest amplification factor, while Rank 7 indicates the highest. The overall ranking score for each lock condition is calculated by summing the ranks across acceleration, velocity, and displacement amplification factors for the four earthquake records.												

Note: Rank 1 represents the lowest amplification factor, while Rank 7 indicates the highest. The overall ranking score for each lock condition is calculated by summing the ranks across acceleration, velocity, and displacement amplification factors for the four earthquake records.

displacement. This approach enables adjustment of the rankings based on the importance of each factor. For instance, when acceleration is a priority, increasing W_a will emphasize configurations that minimize acceleration, while higher values for W_d will prioritize conditions that limit displacement.

This weighted scoring scheme can be summarized by the following formula:

$$\text{Desired ranking levels} = (W_a \times R_{a-\text{rank}}) + (W_v \times R_{v-\text{rank}}) + (W_d \times R_{d-\text{rank}})$$

By varying the weighting factors, different locking conditions may emerge as optimal depending on the priority given to acceleration, velocity, or displacement isolation. For example:

- **If minimizing acceleration is the primary goal**, a higher W_a would prioritize configurations best at reducing acceleration (e.g. L0).
- **If displacement control is critical**, increasing W_d would favor conditions like L4, which minimize displacement.
- **A balanced approach**, as seen in Table 7, uses equal weighting ($W_a = W_v = W_d = 1$), which leads to **L2D** as the optimal configuration with the lowest overall score of 40.

3.2.2. Results

Tables 6 and 7 provide a detailed overview of how different locking conditions influence the amplification of acceleration (R_a), velocity (R_v), and displacement (R_d) of a trolley under four earthquake scenarios. Here is a breakdown of the key insights:

- **L2D** emerges as the most balanced and optimal locking condition, consistently ranking well across acceleration, velocity, and displacement. With the lowest overall ranking score of 40, it stands out as the preferred choice for achieving optimal seismic performance.
- **L1** demonstrates strong performance in isolating acceleration and velocity but can result in significant displacement.
- **L0**, and **L3/L4** exhibit contrasting strengths: **L0** excels at minimizing acceleration but leads to significant displacement, whereas **L3** and **L4** are highly effective in controlling displacement, consistently ranking highest in this category. However, this comes at the expense of poor acceleration control, making them less suitable in situations where managing acceleration is crucial.
- **L2S** and **L2L** tend to be the least favorable choices, receiving the highest overall scores. They provide limited control over velocity and acceleration while also struggling with displacement, particularly under intense ground motions.

These observations indicate the choice of locking condition plays a crucial role in the seismic response of the trolley, with different conditions potentially being more suitable depending on whether the goal is to minimize acceleration, velocity, or displacement. Overall, L2D emerges as a well-balanced option, offering an effective compromise across acceleration, velocity, and displacement.

Table 7 can be developed further by applying a weighting factor between the three parameters, enabling a quantitative approach to assess the trade-off between desired response based on the application.

3.3. Time History Response

Figures 12 and 13 present displacement and rotation time histories of the trolley under various locking conditions subjected to Kobe 100% (GM12) and Christchurch 90% (GM14) earthquake ground motions, respectively. Both figures correspond to scenarios where the trolley angle and wheel angle are set to 0 degrees, and the system is under the "L" self-weight level. In Figure 12, different colors represent different repeats of the same testing conditions.

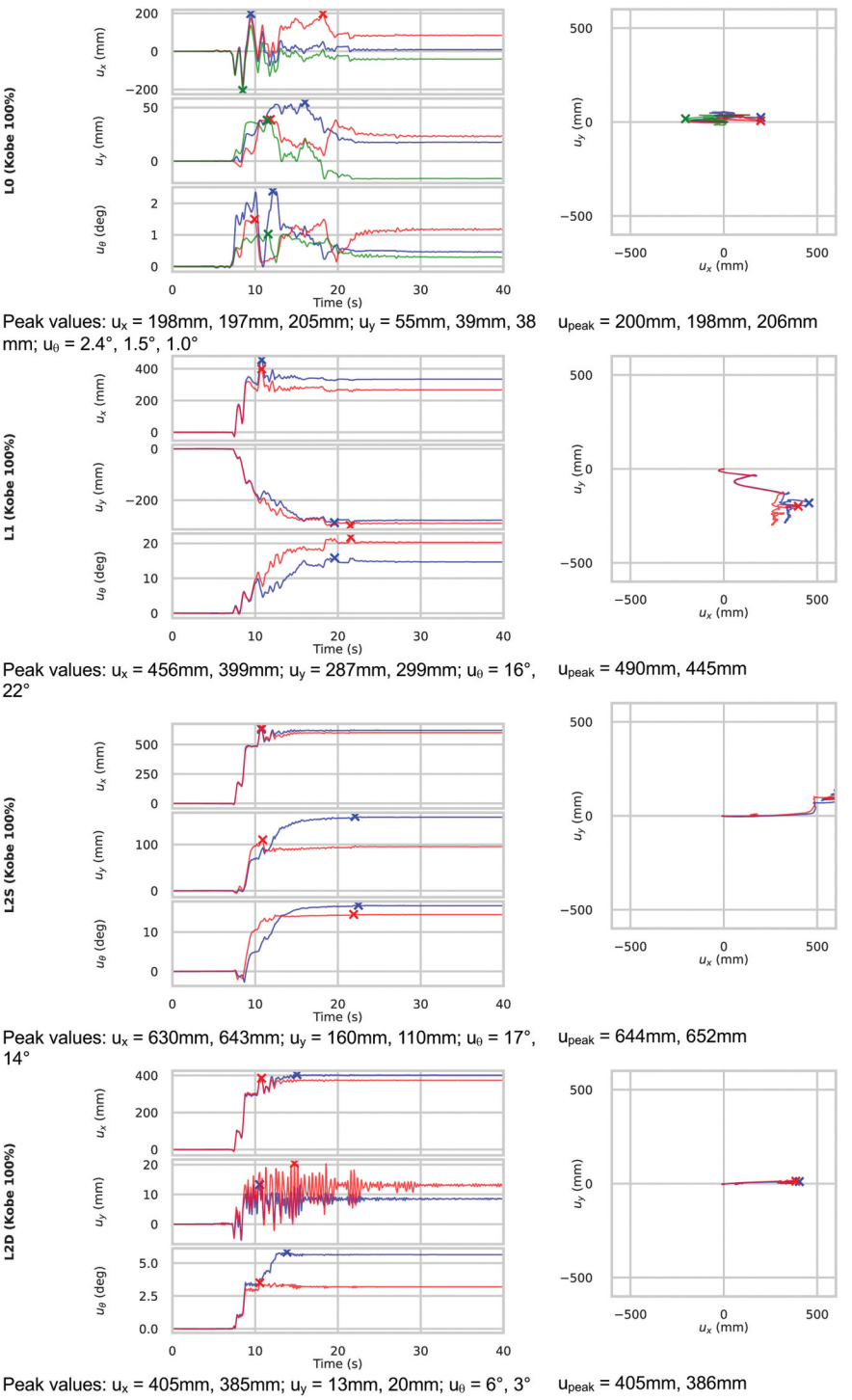

Figure 12. Displacement time history response of the trolley under GM12 - kobe 100%. (a) Responses for lock conditions L0, L1, L2S, and L2D; (b) Responses for lock conditions L2L, L3, and L4, along with the ground motion input.

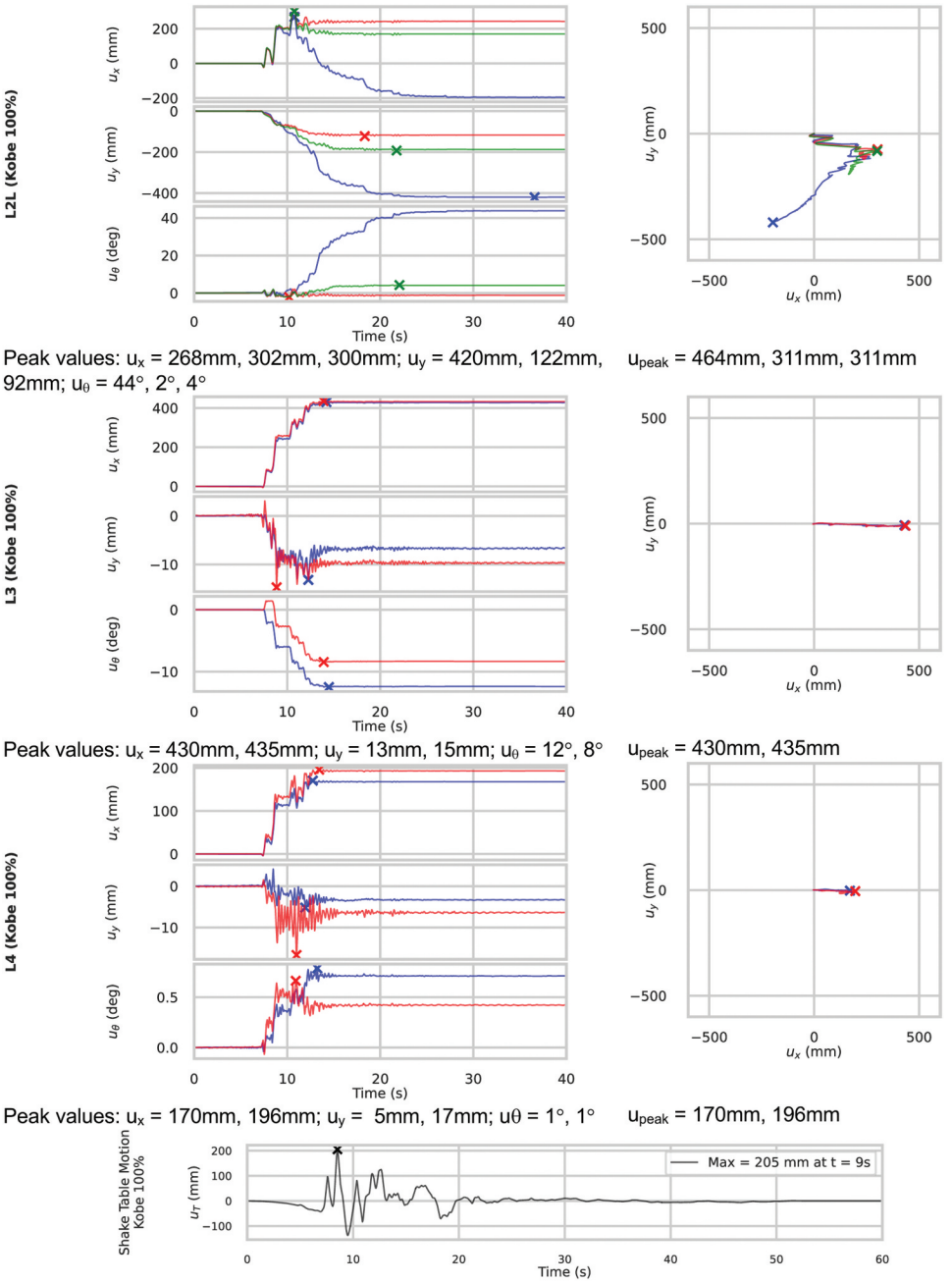

Figure 12. (Continue).

Figures 12 and 13 reveals that:

- Even with a large peak ground displacement (PGD), the Christchurch ground motion (GM14) causes minimal displacement when more than two casters are locked. However, under the L0 free rolling condition, this earthquake results in massive in-plane displacement.

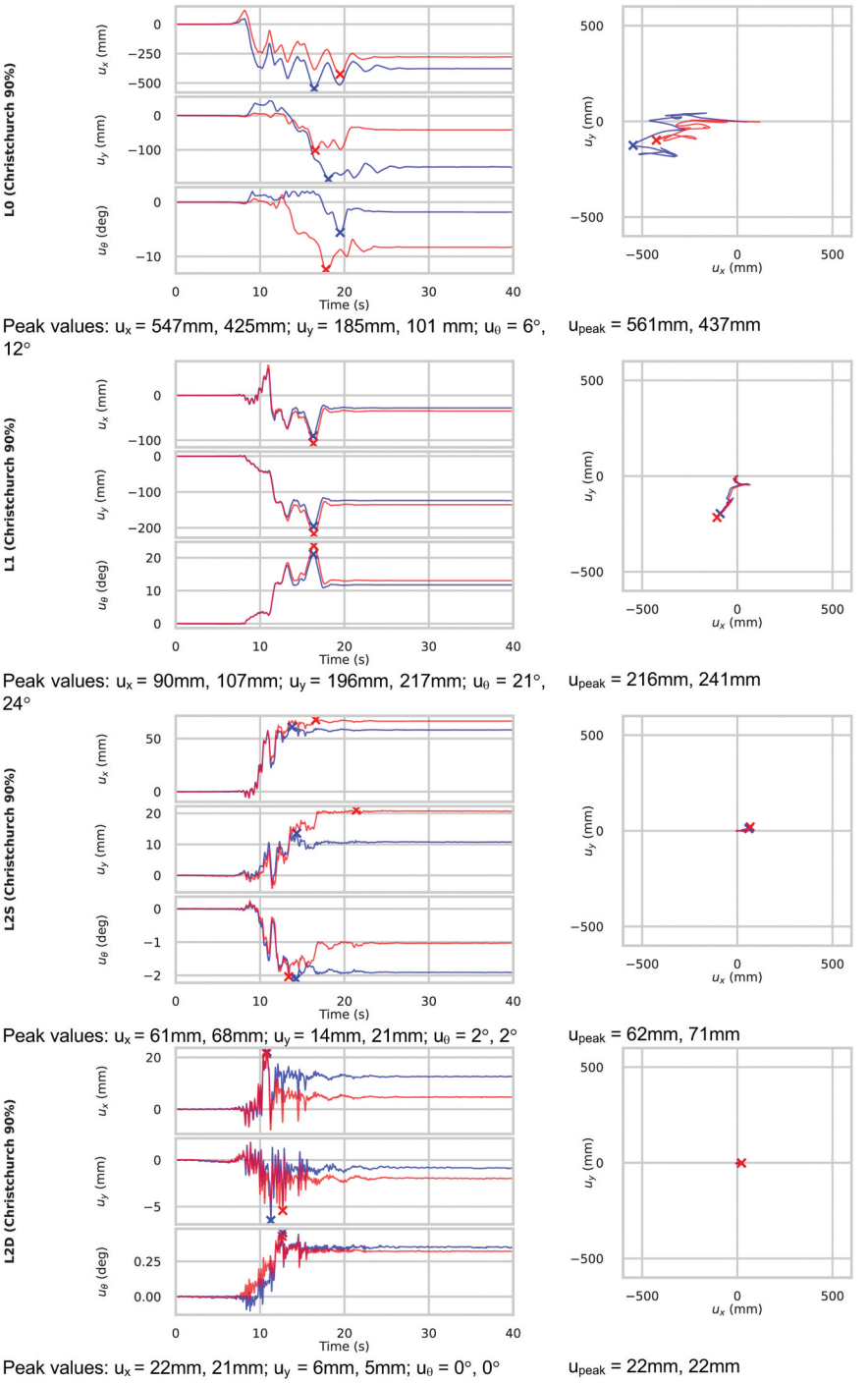

Figure 13. Displacement time history Responses of the trolley under GM14 – Christchurch 90%. (a) Responses for lock conditions L0, L1, L2S, and L2D; (b) Responses for lock conditions L2L, L3, and L4, along with the ground motion input.

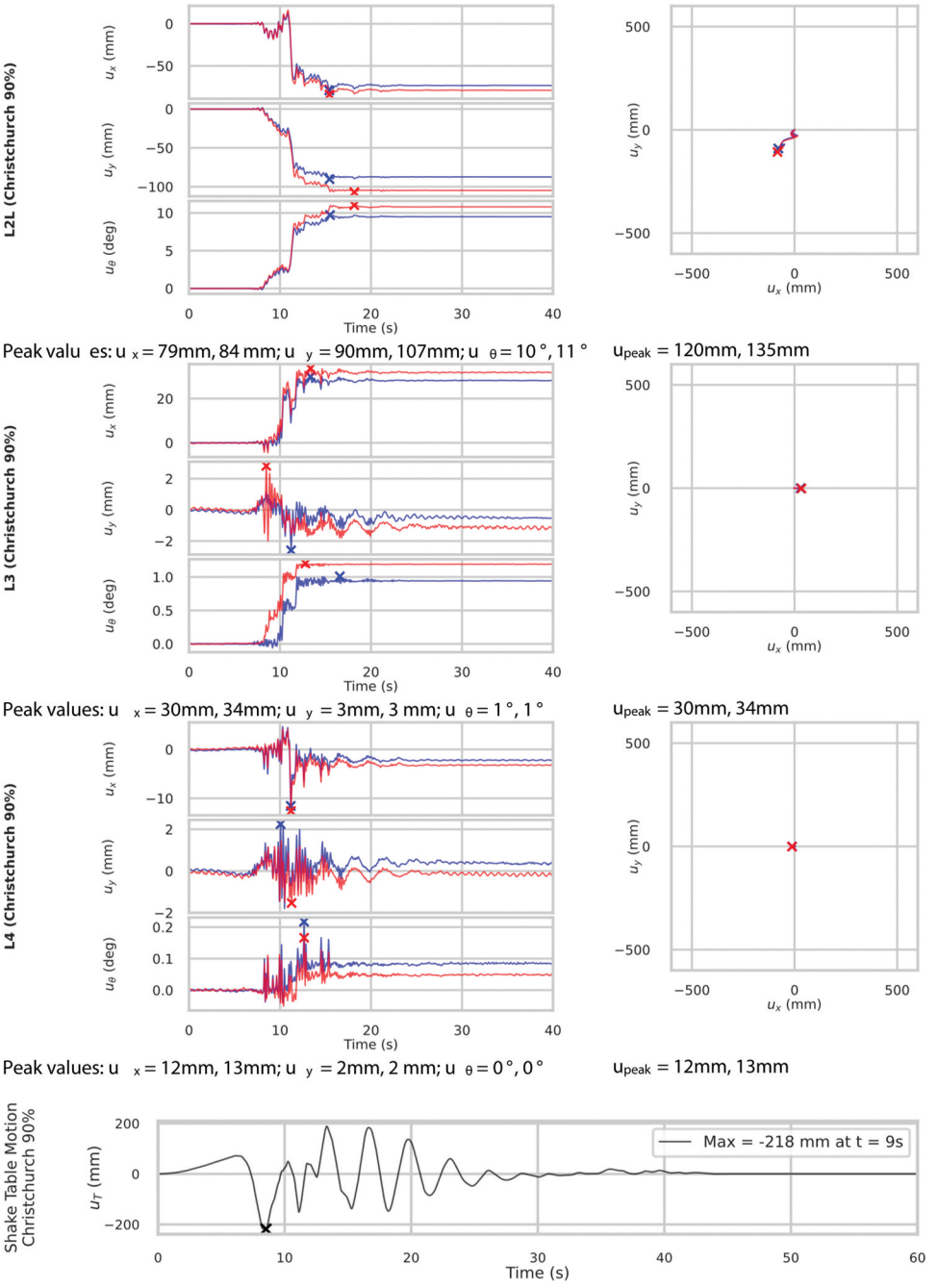

Figure 13. (Continue).

- The Kobe earthquake induces greater displacement and rotational responses across all locking conditions, except for L0, compared to the Christchurch earthquake despite similar PGD.
- L1, L2S, and L2L tend to result in rotation of the trolley, causing it to align obliquely to the ground motion direction. This pattern is evident in both the Kobe and Christchurch earthquakes.

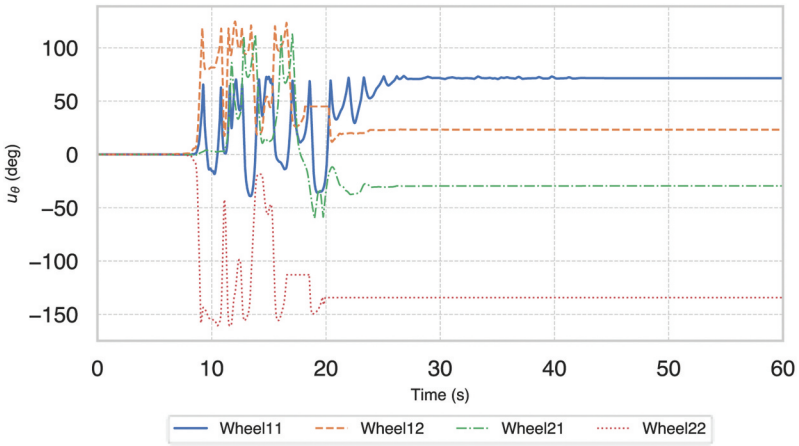

Figure 14. Time history of caster twisting (L0, under GM14 - Christchurch 90%).

- The 2D plan view further demonstrates that the L2D locking condition effectively limits trolley displacement and results in minimal planar rotation compared to other locking conditions.

The time history of caster twisting motion was also recorded, with an example shown in Fig. 14. A detailed analysis of the caster wheel twisting behavior will be presented in a future study. The locations of the four casters are depicted in Fig. 10. The time history response appeared irregular, particularly for the wheels on the mirrored side of the ground motion direction (e.g. Wheel 11 and Wheel 21, as shown in Fig. 10). This irregularity could be attributed to manufacturing differences between wheels, variations in contact areas due to differing wheel heights, or slight discrepancies in the initial trolley position caused by human error.

3.4. Trolley Response Amplification Factors Against Increasing Base Input

3.4.1. Methodology

The seismic response of free-rolling objects differs significantly to fixed objects. It is hypothesized that, due to their lack of restraint and ability to roll freely, free-rolling objects will experience significantly larger displacements, even under relatively minor ground motions. Moreover, their acceleration response is expected to be lower than the ground acceleration, as not all of the seismic forces are transmitted to the object and some energy is dissipated through the rolling motion. Similarly, the velocity response of free-rolling objects is expected to be lower than the ground velocity.

3.4.2. Results

In this section, the response amplification of the trolley as a function of increasing base input is examined. This is achieved by considering data points with same caster types, under varying locking conditions, trolley angles, and ground motion intensity. Figure 15 plots the collated peak trolley unit response against increasing peak base acceleration, peak base velocity and peak base displacement respectively. Each data point in these plots represents the averaged value from six test series, comprising three trolley angles, each repeated twice for a specific caster locking condition and ground motion combination.

Figure 15 reveals the following observations:

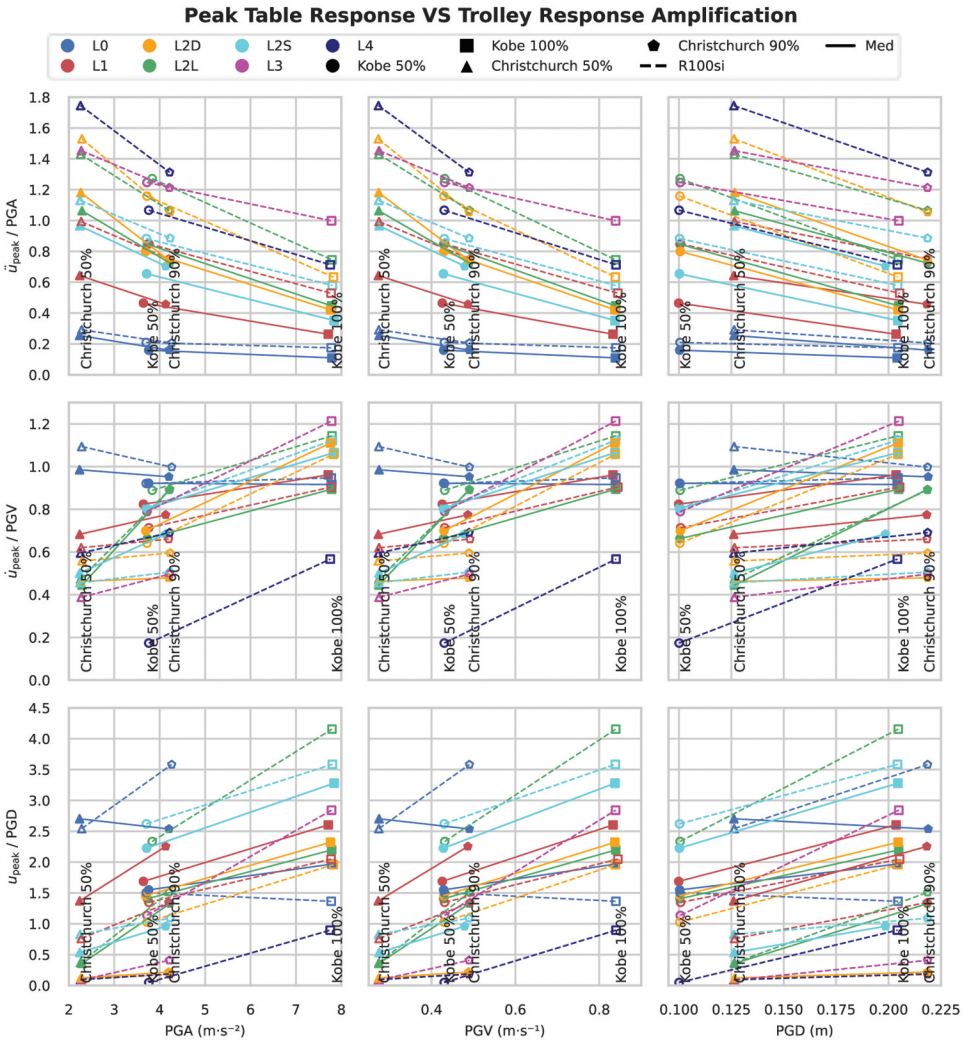

Figure 15. Peak trolley response amplification against increase base input.

1. **Magnitude dependent response amplification:**

Unsurprisingly as base motion increased, the absolute response of the trolley (acceleration, velocity and displacement) also increased. However, valuable insights emerge when examining how the unit response, R (i.e. output/input) changes with increasing base motion. If rolling systems are linear system, then the gradient of the lines in Fig. 15 would be zero. Instead, the trolley response ratio (R) exhibited distinct and consistent non-zero gradients (c) across all locking conditions as peak ground motion (PGM) inputs increase, for each of the acceleration and velocity and displacement response.

A linear relationship can be fitted between response amplification and peak ground motion input, in the form of $R = c \cdot PGM + d$.

- c represents the slope of the linear relationship, indicating how much the response amplification (R) changes per unit increase in peak ground motion (PGM).
- d represents the y-intercept in the linear fit, noting the relationship is empirical and does not correspond to a real amplification value at PGM = 0. In practice, d can be evaluated based on any data point on the linear fit as the slope, c, is fixed and provided.

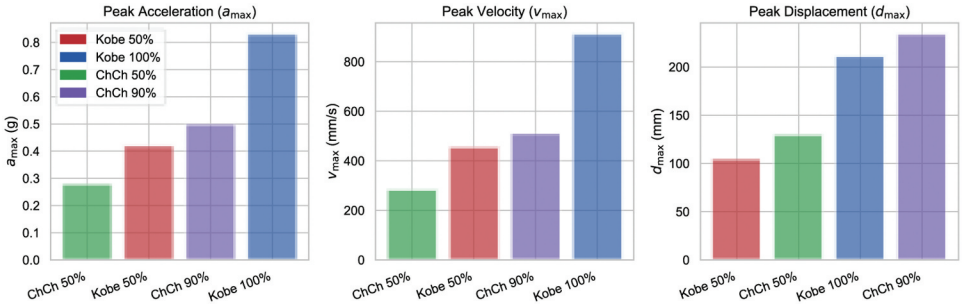

Figure 16. Peak acceleration, velocity, and displacement values of selected ground motions.

The averaged gradients (c) for accelerations, velocity and displacements are as follows:

(1) $\mathbf{c_a} = -0.11$ for acceleration (R_a), standard error: 0.0134
(2) $\mathbf{c_v} = 0.58$ for velocity (R_v), standard error: 0.1203
(3) $\mathbf{c_d} = 6.99$ for displacement (R_d), standard error: 1.0312

The three values represent the averaged gradient values across all lock conditions, both caster types, and all ground motions. These averages are calculated for three specific response ratio categories: PGA vs. Acceleration ratio, PGV vs. Velocity ratio, and PGD vs. Displacement ratio.

This linear relationship provides engineers with a valuable tool for predicting the peak seismic response of rolling equipment based on specific ground motion inputs. Engineers can conduct physical testing at lower intensity ground motion and exploit this linear relationship to accurately determine the maximum response ratio, and thus predict peak response under higher design-level ground motion. This can reduces the cost and complexity of testing but also ensures a reliable forecast of how rolling equipment will respond under design earthquake conditions. This results also demonstrates that the rolling system is nonlinear.

2. **Influence of Ground Motion Record (Kobe vs. Christchurch):**

There are many factors to consider when comparing the influence of different ground motion records, making direct comparisons challenging. This section focuses on the Kobe and Christchurch ground motions (GM11–12 and GM13–14 respectively)

A key point in comparing the Kobe and Christchurch ground motions is that their peak acceleration, velocity, and displacement values differ significantly. For instance, while GM14 (Christchurch 90%) has a similar peak displacement to GM12 (Kobe 100%), this is where the similarity ends. As shown in Fig. 16, the Kobe motion exhibits nearly double higher peak acceleration and velocity. This provides a simple explanation of why Kobe input generally results in larger peak trolley responses.

In the L0 free-rolling condition, Table 6 highlights Christchurch ground motion results in noticeably greater displacement amplification compared to the Kobe motion, while acceleration and velocity amplifications are similar. Then, as the caster locking condition increases (L1 to L4), the Kobe motion leads to higher velocity and displacement amplification and lower acceleration amplification.

This behavior can be partly explained by examining the response spectra of the ground motions, shown in Fig. 17. In the free-rolling state, the trolley behaves like a long-period system. The response spectrum indicates that the Christchurch record contains substantially more energy in the long-period range, making it more prone to displacement amplification. While spectral acceleration in this range is similar for both motions, spectral displacement is markedly higher for Christchurch, which accounts for the large displacement response and amplification for the free rolling trolley.

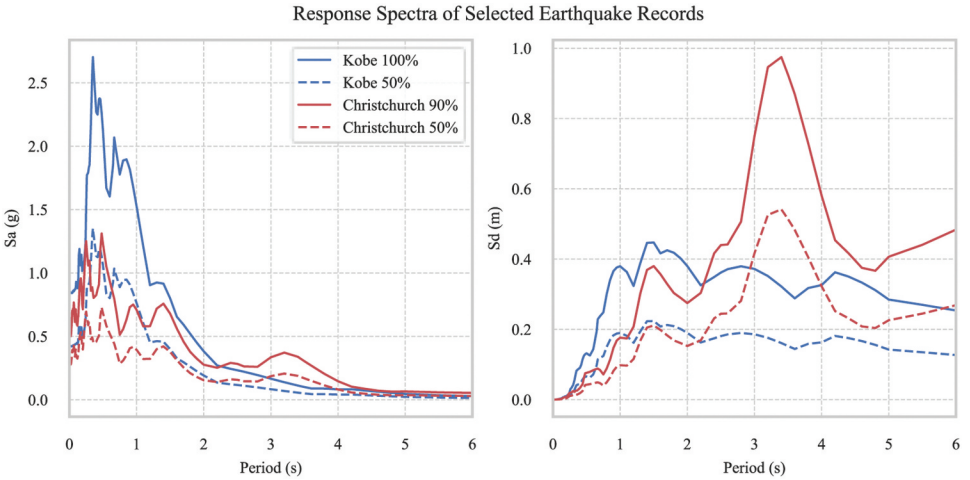

Figure 17. Response spectra of selected ground motions.

For the other caster locking conditions, the system can be approximated as a sliding object with elasto-plastic behavior governed by a variable coefficient of friction (as proposed in Yeow et. al.). As the locking level increases, the secant stiffness of the system also increases, causing the rolling system to behave more like a stiffer structure. As the effective stiffness increases, the system becomes more tuned to the higher frequency range (T_1 < 2 s), where the Kobe ground motion has significantly greater energy content compared to the Christchurch motion, and hence higher response amplification.

4. Research Limitation and Future Work

The primary objective of these shake table tests is to provide benchmark data for validating future simulation techniques. Developing a reliable and accurate simulation method is essential, as it is not feasible to dynamically test every combination of floor configurations, ground motions, and wheel types. It would have been ideal to include a wider range of ground motions in the shake table testing – specifically: (a) sinusoidal ground motions to replicate floor motion, (b) ground motions representative of large earthquakes. However, this was not possible as the trolley response exceeded the safe operating limits of the shake table. (c) While this study does not explicitly consider equipment on floors within buildings, our sinusoidal excitation tests provide relevant insights. In particular, our 1 Hz vibration tests correspond approximately to a fundamental period (T1) of 1s, which is representative of the top floor of a 10-story building. However, locking condition tests did not include sinusoidal ground motion; future research will explore tests incorporating sinusoidal excitations to further investigate their effects. Although the main tests employed earthquake-like excitations, it is acknowledged that equipment located on upper floors would experience motion filtered through the dynamic response of the building. In such cases, the excitation is likely to be more sinusoidal and dominated by the building's natural frequencies, with potential amplification due to resonance. Nevertheless, the observed trends in the effectiveness of different caster locking mechanisms are expected to remain valid. The earthquake-like input revealed fundamental dynamic characteristics of the system: when all casters are free, rolling object behaves as a low-stiffness (long-period) system, and stiffness increases as more casters are locked. These interactions between system flexibility and excitation frequency content are key to understanding the equipment response. The tests presented in this paper provide a significant validation dataset to support the development of numerical models, which will be the subject of future work aimed at evaluating equipment response under a wider range of excitations and

structural conditions. Consequently, this paper focuses on analyzing the response to a select set of ground motions that fall within the capacity of the shaking table, while maintaining a variety of shaking characteristics to support future numerical simulation validation. It is recommended that the conclusions drawn, particularly those related to optimal wheel locking conditions, be interpreted with this limitation in mind. Additional testing at the upper limits of the current capabilities would be beneficial to further validate these findings.

5. Conclusion

The primary objective of this paper is to evaluate seven distinct caster locking configurations under a selected range of table motions. The key findings are as follows:

- **Locking Conditions**: The seismic performance of castered equipment is highly dependent on the chosen locking configuration. The Free-rolling (L0) results in low acceleration but leads to excessive displacement. In contrast, diagonal locking (L2D) offers the best balance between acceleration and displacement, making it the optimal configuration.
- **Caster Types**: Caster selection plays a critical role in stability. Twin-wheel Medical casters outperform single-wheel R100si casters in terms of seismic performance.
- **PGA vs. PGD**: Peak Ground Acceleration (PGA) generally has a more significant impact on trolley response than Peak Ground Displacement (PGD).

These insights hopefully assist medical facilities to improve equipment safety and functionality during seismic events. Specifically, this research finds that choosing the right caster type and locking configuration based on the seismic risks is essential. Adopting optimal setups – such as diagonal locking (L2D) and using twin-wheel medical casters – can substantially enhance the stability and safety of medical equipment, protecting equipment and patients during an earthquake. Healthcare institutions, especially those in seismically active regions, should prioritize these considerations when selecting and maintaining their equipment to mitigate earthquake-related risks.

Acknowledgments

The authors wish to express their sincere gratitude to the technical staff at AUT for their invaluable support during the experimental phase of this research. Special thanks are also extended to the China Scholarship Council for providing the PhD scholarship to the first author.

Author Contributions

CRediT: **Cong Xu:** Conceptualization, Data curation, Formal analysis, Investigation, Methodology, Software, Visualization, Writing – original draft, Writing – review & editing; **Quincy T. Ma:** Conceptualization, Project administration, Resources, Supervision, Writing – review & editing; **Sherif Beskhyroun:** Resources.

Disclosure Statement

No potential conflict of interest was reported by the author(s).

Funding

This work was funded by the China Scholarship Council

ORCID

Cong Xu http://orcid.org/0000-0002-1062-6213
Quincy T. Ma http://orcid.org/0000-0002-9138-8754
Sherif Beskhyroun http://orcid.org/0000-0003-1799-1018
Masahiro Kurata http://orcid.org/0000-0003-1624-1127

Data Availability Statement

The data that support the findings of this study are openly available in Figshare at https://doi.org/10.17608/k6.auckland.27233898.v1.

References

Applied Technology Council. 2015. Performance of Buildings and Nonstructural Components in the 2014 South Napa Earthquake. *FEMA P-1024*. Federal Emergency Management Agency. https://www.atcouncil.org/images/FEMAP-1024_small.pdf.

Baird, A., and H. Ferner. 2017. "Damage to Non-Structural Elements in the 2016 Kaikōura Earthquake." *Bulletin of the New Zealand Society for Earthquake Engineering* 50 (2): 187–193. https://doi.org/10.5459/bnzsee.50.2.187-193.

Chai, J.-F., and F.-R. Lin. 2011. "Seismic Retrofit and Shaking Table Test of Medical Equipment in a Hospital." *Proceedings of the Ninth Pacific Conference on Earthquake Engineering Building an Earthquake-Resilient Society*, Auckland, New Zealand. PCEE. https://www.nzsee.org.nz/db/2011/126.pdf .

Dhakal, R. P. 2010. "Damage to Non-Structural Components and Contents in 2010 Darfield Earthquake." *Bulletin of the New Zealand Society for Earthquake Engineering* 43 (4): 404–411. https://doi.org/10.5459/bnzsee.43.4.404-411.

Dhakal, R. P., A. Pourali, A. S. Tasligedik, T. Yeow, A. Baird, G. MacRae, S. Pampanin, and A. Palermo. 2016. "Seismic Performance of Non-Structural Components and Contents in Buildings: An Overview of NZ Research." *Earthquake Engineering and Engineering Vibration* 15 (1): 1–17. https://doi.org/10.1007/s11803-016-0301-9.

Di Sarno, L., G. Magliulo, D. D'Angela, and E. Cosenza. 2019. "Experimental Assessment of the Seismic Performance of Hospital Cabinets Using Shake Table Testing." *Earthquake Engineering & Structural Dynamics* 48 (1): 103–123. https://doi.org/10.1002/eqe.3127.

Fajfar, P., and H. Krawinkler. 2004. "Performance-Based Seismic Design Concepts and Implementation Proceedings of the International Workshop (no. PEER Report 2004-05)." *International Workshop on Performance Based Seismic Design, Concepts and Implementation, Bled, Slovenia*, Berkeley, CA. Pacific Earthquake Engineering Research Center, University of California.

Filiatrault, A., and T. Sullivan. 2014. "Performance-Based Seismic Design of Nonstructural Building Components: The Next Frontier of Earthquake Engineering." *Earthquake Engineering and Engineering Vibration* 13 (1): 17–46. https://doi.org/10.1007/s11803-014-0238-9.

Guamán-Cabrera, J., J. C. De La Llera, and D. Mery. 2023. "Seismic Performance Assessment of Medical Equipment Using Experimentally Validated Rolling and Toppling Nonlinear Models." *Earthquake Spectra* 39 (3): 1810–1836. https://doi.org/10.1177/87552930231180904.

Mayer, B. J., and M. Boston. 2022. "Advancing NZ Hospital Seismic Readiness: Creating a Post-Earthquake Functionality Dashboard." *NZSEE 2022 Annual Conference*, Wellington, New Zealand. https://www.nzsee.org.nz/wp-content/uploads/2023/03/2022-Conference-Proceedings.pdf.

Miranda, E., G. Mosqueda, R. Retamales, and G. Pekcan. 2012. "Performance of Nonstructural Components During the 27 February 2010 Chile Earthquake." *Earthquake Spectra* 28 (1_suppl1): 453–471. https://doi.org/10.1193/1.4000032.

Mitrani-Reiser, J., M. Mahoney, W. T. Holmes, J. C. De La Llera, R. Bissell, and T. Kirsch. 2012. "A Functional Loss Assessment of a Hospital System in the Bío-Bío Province." *Earthquake Spectra* 28 (1_suppl1): 473–502. https://doi.org/10.1193/1.4000044.

Myrtle, R. C., S. F. Masri, R. L. Nigbor, and J. P. Caffrey. 2005. "Classification and Prioritization of Essential Systems in Hospitals Under Extreme Events." *Earthquake Spectra* 21 (3): 779–802. https://doi.org/10.1193/1.1988338.

Nikfar, F., and D. Konstantinidis. 2019. "Experimental Study on the Seismic Response of Equipment on Wheels and Casters in Base-Isolated Hospitals." *Journal of Structural Engineering* 145 (3): 04019001. https://doi.org/10.1061/(ASCE)ST.1943-541X.0002266.

OptiTrack. 2023. "Motive." *Computer Software*. https://optitrack.com/software/motive/.

Ornthammarath, T., and T. Puavaranukroh. 2018. "Observed Hospital Damages Following the 2014 Mae Lao (Northern Thailand) Earthquake: A Survey Report." *Journal of Disaster Research* 13 (4): 804–812. https://doi.org/10.20965/jdr.2018.p0804.

Pantoli, E., X. Wang, M. Chen, T. Hutchinson, B. Meacham, and H. J. Park. 2013. "Shake Table Testing of a Full-Scale Five-Story Building: Performance of the Major Nonstructural Components - Egress and façades." *Structures Congress* 2013:1447–1459. https://doi.org/10.1061/9780784412848.128.

Suzuki, Y., I. Fukuda, and S. Nakaji. 2014. "The Operating Room During a Severe Earthquake: Lessons from the 2011 Great East Japan Earthquake." *Disaster Medicine and Public Health Preparedness* 8 (2): 123–129. https://doi.org/10.1017/dmp.2014.16.

Taghavi, S., and E. Miranda. 2003. Response Assessment of Nonstructural Building Elements—Peer Report. Pacific Earthquake Engineering Research Center (PEER). https://peer.berkeley.edu/publications/2003-05.

Wang, D., J. Dai, and X. Ning. 2016. "Shaking Table Tests of Typical B-Ultrasound Model Hospital Room in a Simulation of the Lushan Earthquake." *Bulletin of the New Zealand Society for Earthquake Engineering* 49 (1): 116–124. https://doi.org/10.5459/bnzsee.49.1.116-124.

Yeow, T. Z., G. A. MacRae, R. P. Dhakal, and B. A. Bradley. 2018. "Validating the Sliding Mechanics of Office-Type Furniture Using Shake-Table Experiments." *Bulletin of the New Zealand Society for Earthquake Engineering* 51 (1): 1–11. https://doi.org/10.5459/bnzsee.51.1.1-11.

Zhang, L., X. Liu, Y. Li, Y. Liu, Z. Liu, J. Lin, J. Shen, X. Tang, Y. Zhang, and W. Liang. 2012. "Emergency Medical Rescue Efforts After a Major Earthquake: Lessons from the 2008 Wenchuan Earthquake." *The Lancet* 379 (9818): 853–861. https://doi.org/10.1016/S0140-6736(11)61876-X.

Zito, M., R. Nascimbene, P. Dubini, D. D'Angela, and G. Magliulo. 2022. "Experimental Seismic Assessment of Nonstructural Elements: Testing Protocols and Novel Perspectives." *Buildings* 12 (11): 1871. https://doi.org/10.3390/buildings12111871.